Electrochimica Acta 258 (2017) 1160–1172

Contents lists available at ScienceDirect

Electrochimica Acta

journal homepage: www.elsevier.com/locate/electacta

Determination of standard redox rate constants of OLED active compounds by electrochemical impedance spectroscopy

Pavel Chulkin [a], Mieczyslaw Lapkowski [a, b], Martin R. Bryce [c], Jose Santos [c], Przemyslaw Data [a, b, d, *, 1]

[a] Silesian University of Technology, Faculty of Chemistry, Department of Physical Chemistry and Technology of Polymers, 44-100 Gliwice, Strzody 9, Poland
[b] Centre of Polymer and Carbon Materials of the Polish Academy of Sciences, Zabrze, Poland
[c] Durham University, Department of Chemistry, South Road, DH1 3LE, Durham, United Kingdom
[d] Durham University, Department of Physics, South Road, DH1 3LE, Durham, United Kingdom

ARTICLE INFO

Article history:
Received 12 August 2017
Received in revised form
5 November 2017
Accepted 23 November 2017
Available online 24 November 2017

Keywords:
OLED
Standard redox rate constant
Electrochemical impedance spectroscopy
Donor
Acceptor
Ambipolar
Exciplex
TADF

ABSTRACT

A number of commercial organic compounds (m-MTDATA, PBD, CBP, TAPC, NPB, TPBi, etc) as well as several donor-acceptor-donor (D-A-D) compounds were investigated by cyclic voltammetry and electrochemical impedance spectroscopy. The compounds were chosen as they are promising components of small-molecule-based high efficiency Thermally Activated Delayed Fluorescence (TADF) emitters in Organic Light Emitting Diodes (OLEDs).

Electrochemical impedance spectra of a Pt electrode in CH_2Cl_2 solutions containing the investigated compound and Bu_4NBF_4 as the electrolyte were obtained and analyzed by electrochemical electrical circuit methods. Charge transfer resistance, double layer capacitance, Warburg constant and other parameters were determined and represented as a function of the potential. Analysis of charge transfer resistance as a function of potential allowed an estimation of standard redox rate constants for the compounds' oxidation and reduction processes.

Two main features concerning the redox reaction rates of OLED-active compounds were revealed: (i) the oxidation and reduction rates of ambipolar compounds, i.e. containing both donor and acceptor parts, were found to be much higher than those of unipolar donor-only and acceptor-only molecules; (ii) the relationship between the oxidation and reduction rate constants was shown to be related to the compounds' conductivity type in the solid state.

1. Introduction

Nowadays one of the most interesting applications of organic compounds is in the rapidly expanding organic electronics area [1]. A common theme in organic electronics is that the organic compounds need to function in an environment where an electric current is passed through them, so whether the compound is a conductor, semi-conductor or insulator, the electrochemical investigation is necessary. Electrochemical methods are usually applied at the first stage of characterisation of the organic compounds. There are several different electrochemical methods which can be used to analyse organic compounds but the mostly widely used one is Cyclic Voltammetry (CV). The main goal of a CV investigation is determination of the compound's stability and an estimation of the Ionization Potential (IP) and Electron Affinity (EA) which correspond to the Highest Occupied and Lowest Unoccupied Molecular Orbital (HOMO and LUMO) energy levels, respectively [2–13]. From an organic electronics point of view, the energy levels are an important criterion for device design, since they determine energy losses during charge transfer across the layer-layer interfaces. They also determine exciplex formation and its emission energy.

In this study we developed an electrochemical impedance-based technique for estimation not only of thermodynamic but also of kinetic parameters of molecular oxidation and reduction processes. Analysis of electrochemical impedance spectra has

* Corresponding author. Silesian University of Technology, Faculty of Chemistry, Department of Physical Chemistry and Technology of Polymers, 44-100 Gliwice, Strzody 9, Poland; Durham University, Department of Physics, South Road, DH1 3LE, Durham, United Kingdom.
E-mail addresses: Przemyslaw.Data@durham.ac.uk, Przemyslaw.Data@polsl.pl (P. Data).
[1] ISE member.

https://doi.org/10.1016/j.electacta.2017.11.171

Table 1
Standard electrochemical rate constants, structures and roles of a number of commercial OLED compounds.

	Structure	E_{EA} [eV]	E_{IP} [eV]	k^0_{red} [m/s]	k^0_{ox} [m/s]	Use in OLEDs
m-MTDATA	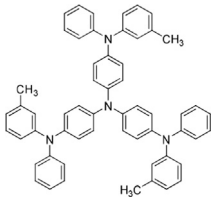	−2.0	−5.1	–	$1.4\cdot10^{-3}$	donor, hole-transport layer [16]
CBP	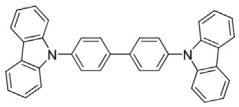	−2.9	−6.0	–	–	host, hole-transport layer [11]
tBu-PBD	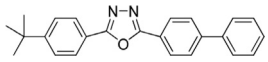	−2.6	−6.2	$7.3\cdot10^{-5}$	–	acceptor, electron-transport layer [17]
NPB	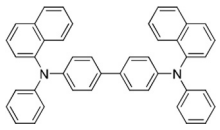	−2.4	−5.4	–	$8.7\cdot10^{-4}$	donor, hole-transport layer [14]
TPBi	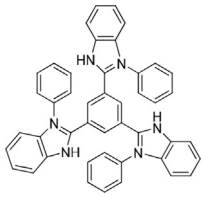	−2.7	−5.9	$1.2\cdot10^{-5}$	–	acceptor, electron-transport layer [14]
TAPC	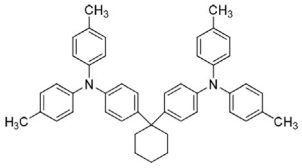	−2.0	−5.2	–	$2.5\cdot10^{-3}$	donor, hole-transport layer [10]
3TPYMB	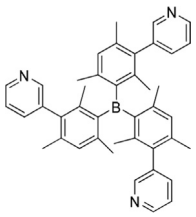	−3.3	−6.8	–	–	acceptor, electron-transport layer [16]
mCP	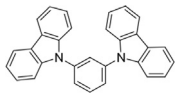	−2.4	−6.1	–	–	host, hole-transport layer [18]
DPEPO	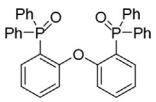	−2.0	−6.1	–	–	host[15]
CzSi	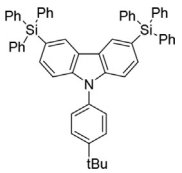	−2.5	−6.0	–	–	host[19]

enabled the extraction of purely kinetic parameters, charge transfer resistance, which value is not affected by diffusion.

Our new method includes the following stages. Firstly, potential regions corresponding to reversible oxidation and reduction processes are revealed by cyclic voltammetry. Then a number of impedance spectra in increments of 0.1 V are registered in the potential range where a reversible peak is observed in the CV. All the spectra are analysed by an equivalent electrical circuit method,

Table 2
Standard electrochemical rate constants of a number of D-A-D OLED compounds and estimated values of their HOMO and LUMO levels.

	Structure	LUMO, eV	HOMO, eV	k^0_{red}, m/s	k^0_{ox}, m/s
I	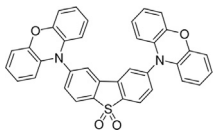	−3.15	−5.61	$3.7\cdot10^{-4}$	$4.6\cdot10^{-3}$
II	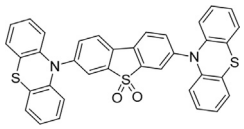	−3.03	−5.56	$1.4\cdot10^{-4}$	$1.8\cdot10^{-3}$
III	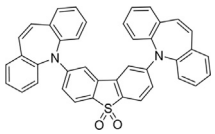	−2.55	−6.04	$2.3\cdot10^{-4}$	$1.1\cdot10^{-4}$
IV	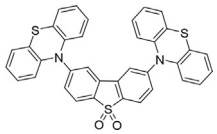	−3.08	−5.62	$1.9\cdot10^{-4}$	$> 1\cdot10^{-3}$
V	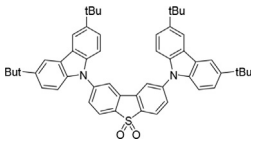	−2.97	−6.07	$4.3\cdot10^{-3}$	$9.4\cdot10^{-4}$
VI	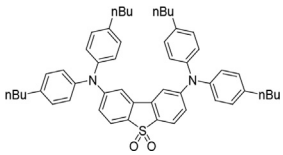	−2.7	−5.83	$7.6\cdot10^{-3}$	$8.4\cdot10^{-4}$

and the parameters (resistance, capacitance, etc) are presented as functions of potentials, and the electrochemical rate constant is calculated.

For our work 10 commercial compounds were chosen: 4,4′,4″-Tris[phenyl(*m*-tolyl)amino]triphenylamine (**m-MTDATA**); 4,4′-Bis(*N*-carbazolyl)-1,1′-biphenyl (**CBP**); 2-(4-*tert*-butylphenyl)-5-(4-biphenylyl)-1,3,4-oxadiazole (**tBu-PBD**); *N,N*′-Di(1-naphthyl)-*N,N*′-diphenyl-(1,1′-biphenyl)-4,4′-diamine (**NPB**); 2,2′,2"-(1,3,5-Benzinetriyl)-tris(1-phenyl-1-*H*-benzimidazole) (**TPBi**); 4,4′-Cyclohexylidenebis[*N,N*-bis(4-methylphenyl)benzenamine] (**TAPC**); 1,3-Bis(*N*-carbazolyl)benzene (**mCP**), Tris(2,4,6-trimethyl-3-(pyridin-3-yl)phenyl)borane (**3TPYMB**); Bis[2-(diphenylphosphino)phenyl] ether oxide (**DPEPO**); 9-(4-*tert*-butylphenyl)-3,6-bis(triphenylsilyl)-9*H*-carbazole (**CzSi**) mostly to show the usefulness of the method. These compounds were chosen because they take an active part in intermolecular exciplex formation (Table 1) [10,12,14,15].

To expand our work, several ambipolar compounds consisting of both donor and acceptor parts (D-A-D) were also studied (Table 2): 2,8-bis(10*H*-phenoxazin-10-yl)dibenzo[*b,d*]thiophene-*S,S*-dioxide (**I**) (see supporting information for details); 3,7-bis(10*H*-phenothiazin-10-yl)dibenzo[*b,d*]thiophene-*S,S*-dioxide (**II**) [8]; 2,8-bis(5*H*-dibenzo[*b,f*]azepin-5-yl)dibenzo[*b,d*]thiophene-5,5-dioxide (**III**) see supporting information for details); 2,8-bis(10*H*-phenothiazin-10-yl)dibenzo[*b,d*]thiophene-*S,S*-dioxide (**IV**) [8,9]; 9-[2,8]-9-carbazole-[dibenzothiophene-*S,S*-dioxide]-carbazole (**V**) [10]; 2,8-bis(bis(4-butylphenyl)amino)dibenzo[*b,d*]thiophene-5,5-dioxide (**VI**) [11].

2. Experimental section

Structural formulas of the compounds are provided in Tables 1 and 2 along with a summary of the results obtained. Commercial compounds (Table 1) were purchased from Sigma-Aldrich, TCI or Molekula and used without further purification. The working CH_2Cl_2 solution in all experiments contained $5\cdot10^{-3}$ mol/L of the investigated organic compound and 0.1 mol/L Bu_4NBF_4 as an electrolyte. The solution was initially deaerated by Ar for 10 min, and the atmosphere above the solution was saturated with Ar during whole measurement procedure.

The electrochemical experiments were carried out using a Bio-Logic SP-150 potentiostat with a built-in frequency response analyser. Pt working electrode ET075 from eDAQ, Pt counter electrode (wire) and Ag/AgCl reference electrode were employed in a three-electrode electrochemical cell. The counter electrode was flame annealed and the working electrode was polished before each experiment. All the potentials in this work are presented versus Fc^+/Fc (ferrocene) reference potential.

The potential scan rate used in cyclic voltammetry was 100 mV/s. Impedance spectra were obtained in the 10 kHz−1 Hz frequency range with 20 points per decade in a logarithmic scale (total number of frequencies in one spectrum was 61). The analysis of the electrochemical impedance spectra and the determination of equivalent circuit parameters was performed using « EIS

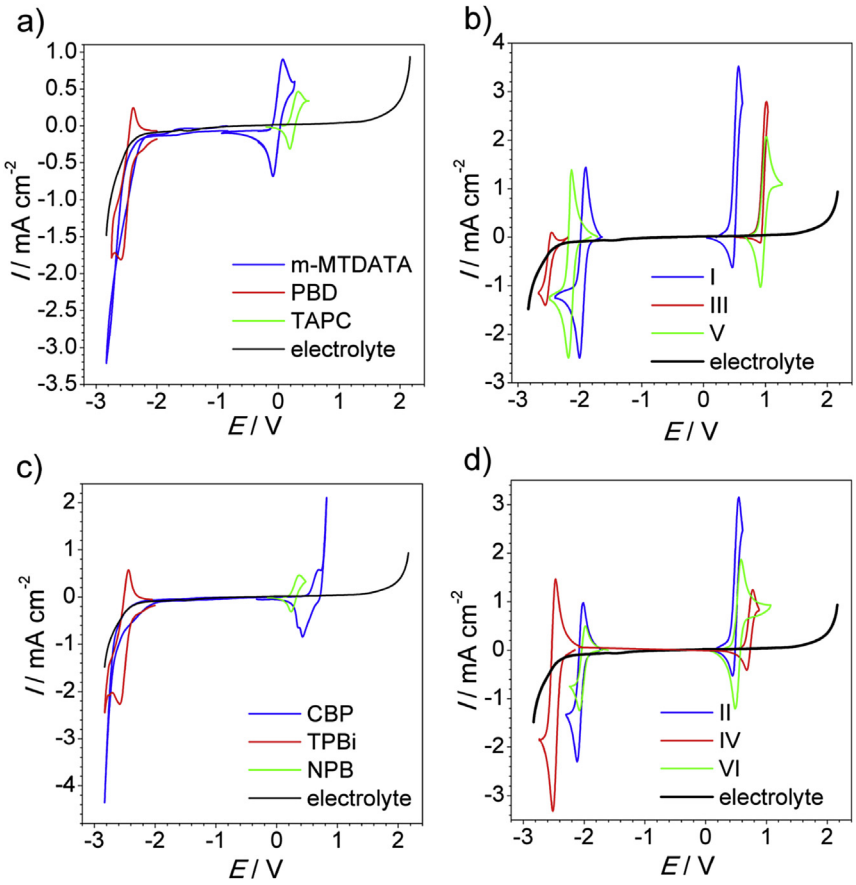

Fig. 1. Characteristic cyclic voltammograms showing oxidation and reduction of the compounds. Sample concentration 0.05 M, scan rate 0.05 V s^{-1}, dichloromethane solution. All potentials vs Fc/Fc^{+} redox couple.

Analyser » software [20].

3. Results and discussion

The characteristic voltammetric peaks of the compounds in solution are shown in Fig. 1 in comparison with background current of the solvent and electrolyte. The background current significantly complicated recognition of reduction peaks, especially in case of compounds enlisted in Table 1, however in order to maintain the same condition throughout the work we did not refuse of using dichloromethane which appeared to be the best to dissolve all the compounds under investigation up to concentration of 0.05 M required for characterisation of the redox kinetics. The oxidation peaks of the compounds appeared in a range of 0–1.3 V while reduction peaks were observed in a range between −1.7 and −2.5 V.

As Fig. 1 a, c shows that most compounds enlisted in Table 1 underwent either oxidation (m-MTDATA, TAPC, NPB) or reduction (PBD, TPBi) over a broad potential range. Several compounds (DPEPO, CzSi, mCP, 3TPYMB) did not show any noticeable redox behaviour. Since oxidation of all the compounds occurred at rather low potentials (<1 V) electrolyte oxidation did not mask them and complicate estimation of oxidation potential. CVs of TPBi and PBD did not show any significant difference in comparison with the background curve in broad positive potential range, thus they were considered non-oxidisable.

Two compounds (NPB and TAPC) did not show any noticeable reduction behaviour. Nevertheless a considerable cathodic current within the range of supposed reduction potentials in case of CBP and m-MTDATA was observed. In first experiments involving very high scan rate (up to 0.2 V s^{-1}) and high electrolyte concentration (up to 1.0 M) we observed a small anodic current peak right after the switch of the scan direction which was initially wrongly recognised as a part of quasi-reversible reduction process peak. Supposing that the current responsible for compound reduction may overlap with masking background current, we tried to characterise the reduction process by impedance method anyway within the range of possible reduction potential calculated from reference data about LUMO levels. Finally, no reduction process could be detected and characterised.

The narrow peak potential regions (Fig. 1 b, d) of the D-A-D compounds enlisted in Table 2 enabled an estimation of the IP and EA levels, as well as selection of the ranges for registering the impedance spectra. A potential range with a 0.2 V width including a redox peak was chosen and 21 spectra were obtained at 0.01 V increments.

The only reliable information we could certainly extract from CVs were estimated positions of the redox peaks and qualitative description of reversibility of the process. The non-equality of oxidation and reduction peaks observed for **III**, **IV** and **VI** (Fig. 1 b, d) could not be explained by effect of one single factor. Voltammetric peaks are known to be affected by a set of inseparable factors such as number of electrons transferred, transfer coefficient (α), charge transfer (Faraday process) rate, diffusion of the species and side processes involving reactants, products and other solution components. Registration of characteristic peak was a tricky challenge since immediately after first reversible process all the compounds were found to undergo irreversible redox transformation

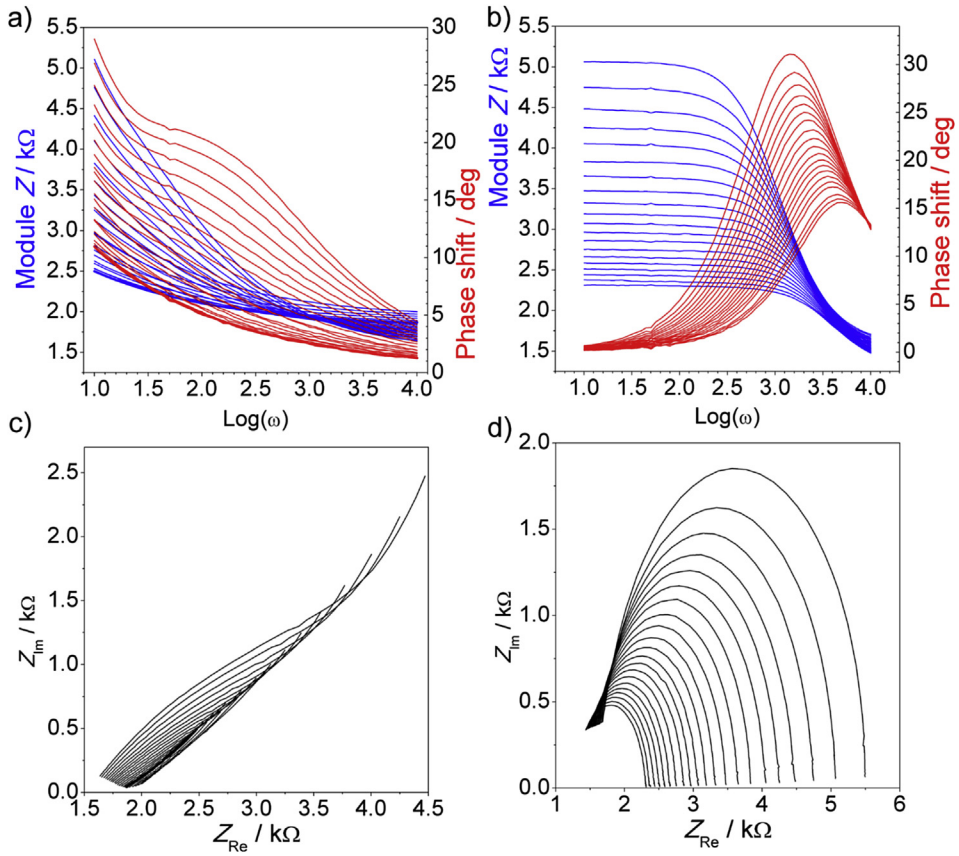

Fig. 2. Bode (a, b) and complex plane plots (c, d) of **m-MTDATA** impedance spectra in oxidation (a, c) and reduction (b, d) potential ranges. Impedance spectra were registered in increments of 0.01 V in the ranges +0.03 – +0.23 V (oxidation) and −2.7 – −2.9 V (reduction). The thick lines corresponds to oxidation equilibrium potential +0.08 V (a, c).

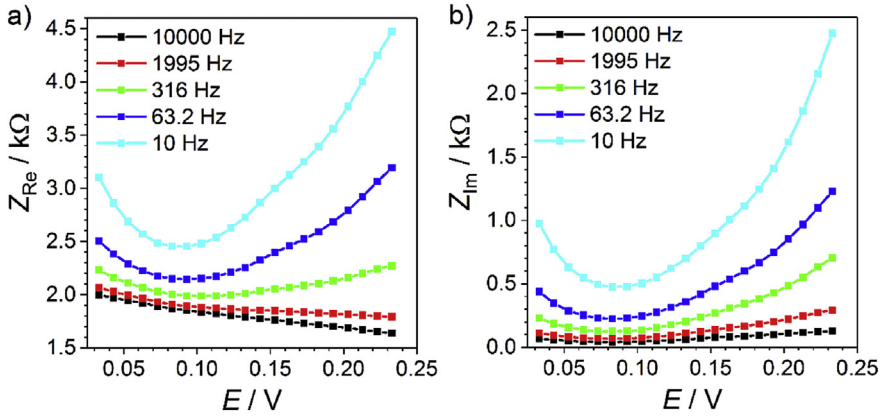

Fig. 3. Real and imaginary impedance as functions of electrode potential corresponding to **m-MTDATA** reversible oxidation (Fig. 2 a, c) versus the potential at five selected frequencies.

accompanied by electrode surface blocking and preventing consequent registration of a reverse scan.

A considerably high solution resistance was a problem usually concomitant with organic solvents. The effect was confirmed by impedance spectroscopy which allowed evaluation of system potential-independent resistance as will be shown below. That fact along with irreversibility disabled direct estimation of number of electrons transferred in one step from the peak potential difference, which equals 0.059/z (V) in case of reversible process and zero ohmic ($I \cdot R$) potential drop in solution.

Fortunately impedance spectra analysis, potential dependence charge transfer resistance plots in particular, allowed determination of z value, which was found to be equal to 1 for all the processes considered. Moreover molecular structures of the compounds do not imply possibility of one-step oxidation to bication, that is relatively more stable than preceding radical-cation, as happens in case of symmetrical conjugated compounds (e.g. anthraquinone).

Because of the large number of investigated compounds and the similarity of their impedance spectra we will show and thoroughly discuss the spectra of oxidation of the popular donor **m-MTDATA,** reduction of acceptor and electron transfer material **TPBi** and both redox processes that involve emitter **V** (D-A-D compound) that is established as a promising component in the emission layer for

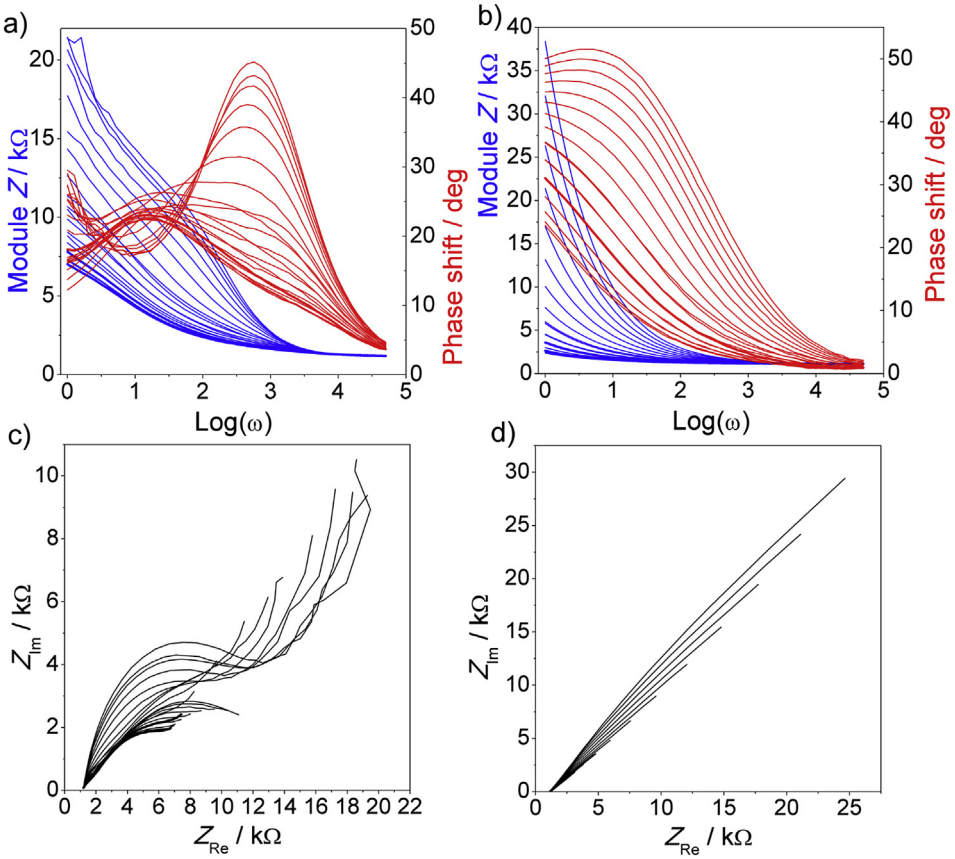

Fig. 4. Bode plots (a, b) and complex plane plots (c, d) of impedance spectra of **V** in reduction (a, c) and oxidation (b, d) potential ranges. Impedance spectra were registered in increments of 0.01 V in the ranges +0.83 – +1.03 V (oxidation) and −2.05 – −2.25 V (reduction). The thick lines correspond to equilibrium potentials: −2.13 V for reduction (a, c) and +0.97 V for oxidation (b, d).

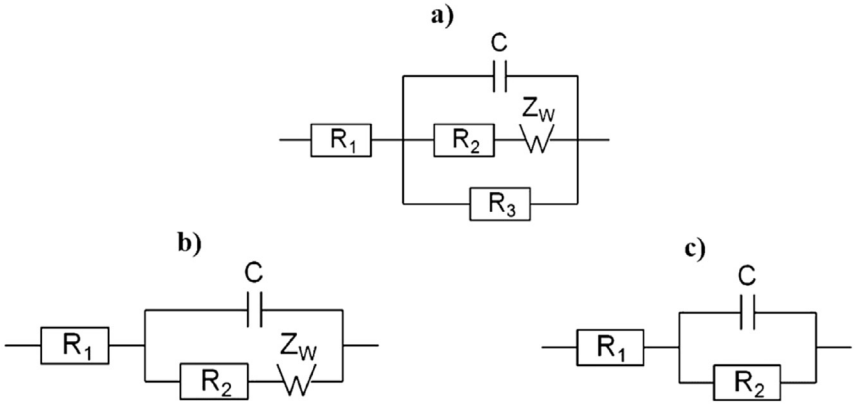

Fig. 5. Equivalent electric circuits derived to fit the experimental spectra.

OLEDs [10].

The CV of **m-MTDATA** showed a reversible oxidation peak at ca. 0.1 V and no obvious reduction process was observed (Fig. 1 a). However we will still consider voltage range −2.7 – −2.9 V as an example of treatment of irreversible process and attempt to describe kinetics of a process masked by high background current. During potential scanning in the positive direction in the 0.03–0.23 V range (Fig. 2a,c) both real and imaginary parts decrease until 0.08 V is reached and then start increasing until the end of the scan. Since both real and imaginary parts are minimal at the equilibrium potential, so is the impedance module.

The Bode plot (Fig. 2 a) clearly shows minimization of the impedance at +0.08 V, i.e. at an equilibrium potential, as will be proved below. The phase shift is also minimal at this potential. However, this is not compulsory, as there are no definite kinetic reasons for such a behaviour of the phase shift. A double layer capacitance that affects the imaginary part is controlled by other independent processes. Minimization of the phase shift at the equilibrium potential was a coincidence observed for several compounds including **m-MTDATA**. The evolution of both values of the real and imaginary impedance during potential scanning in the oxidation peak region is shown in Fig. 3.

As was proposed by CV analysis, the reduction of **m-MTDATA** is either irreversible or doesn't take place at all. During potential

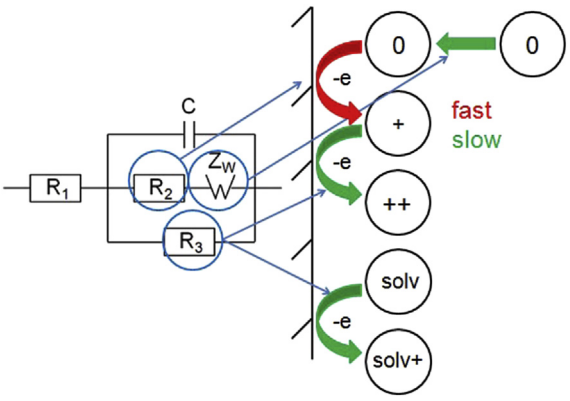

Fig. 6. Correspondence of equivalent electric circuit to the proposed schematic mechanism of the electrochemical processes. Fast and slow stages are assigned by red and green arrows, respectively. (For interpretation of the references to colour in this figure legend, the reader is referred to the web version of this article.)

scanning in the negative direction in the −2.7 – −2.9 V range (Fig. 2 b,d) a consecutive decrease of impedance is observed without intermediate impedance minima.

The shown example depicts two ways of treatment stipulated by the reversibility of a process. When the process is purely reversible then there is a potential at which the rates of forward and backward redox processes are equal. Then the impedance is minimal and the equilibrium potential can be determined by both CV and EIS methods, the latter being a tool to estimate the rate constant. If the process is irreversible then only the forward electrochemical process is observed and its rate increases monotonically with the potential. In that case there is no distinctive point on the plot and the potential at the start of the current growing is regarded as the redox equilibrium potential. Nevertheless, the rate constant can still be determined from impedance data, but its value would be strongly dependent on the accepted value of the equilibrium potential.

The impedance spectra of **V** shown in Fig. 4 are typical of compounds with both reversible oxidation and reduction profiles. In both cases the impedance passes through a minimum as the potential is scanned in a peak interval. Bode plots (Fig. 4b,d) are useful to represent that kind of spectral evolution. The thick lines in both figures (Fig. 4b,d) correspond to the equilibrium potential that lies in the middle of the scanning interval. As stated above, the phase shift is not always minimal at the equilibrium potential. That means that minimums on the real and imaginary potential plots do not always coincide, because they may be affected by different processes that occur at the electrode-solution interface.

3.1. Impedance spectra analysis

An equivalent electrical circuit shown in Fig. 5 a was found to fit all the experimental spectra obtained in this work. In some cases its simplified modifications (Fig. 5b and c) could be used.

The proposed mechanism describing the equivalent circuit (Fig. 5a) is illustrated in Fig. 6. Impedance corresponding to diffusion of a neutral molecule to the electrode surface is described by a specific Warburg element (W). The molecule approaching the electrode surface undergoes fast oxidation (as shown as an example

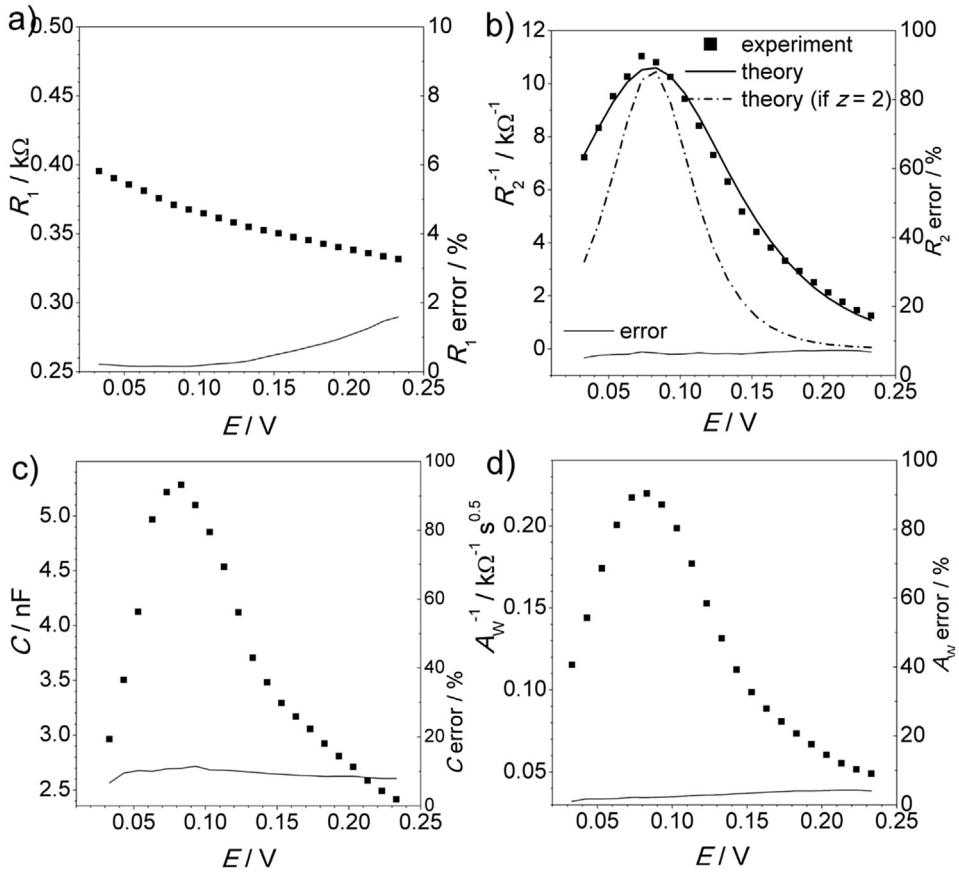

Fig. 7. Equivalent circuit parameters: R_1 (a), R_2^{-1} (b), C (c), A_W^{-1} (d), their errors and fitting theoretical curves (b) corresponding to **m-MTDATA** oxidation as functions of electrode potential.

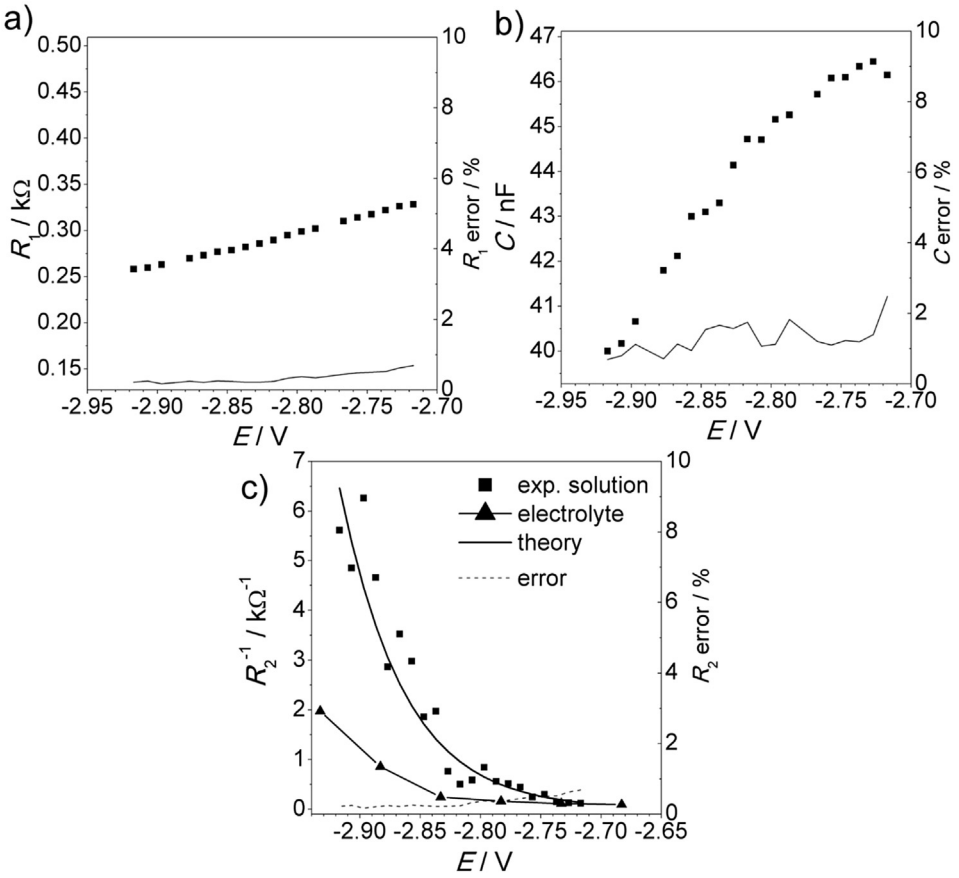

Fig. 8. Equivalent circuit parameters: R_1 (a), C (b), R_2^{-1} (c), determined within the range −2.7 to −2.9 V in presence of **m-MTDATA**. A background curve of charge transfer conductivity obtained for electrolyte solution and theoretical fitting is shown (c).

in Fig. 6) or reduction described by the charge transfer resistance (R_2). Consequently the oxidised molecule may undergo further oxidation or reduction. This stage does not determine the rate of the first oxidation process. Therefore, it is represented by a parallel charge path comprising charge transfer resistance (R_3). The other side-processes, such as solvent oxidation or reduction, contribute to the parallel charge transfer path. Since frequency responses of two parallel resistors are indistinguishable, all relatively slow charge transfer processes are described by one element (R_3). The element of capacitance (C) characterises a double electric layer. Its value is not related directly to the kinetics of the redox process so this element will not be considered in further discussions. The element of resistance (R_1) characterises charge transfer besides the electrode-electrolyte interface, i.e. solution and electrodes.

The rates of the processes (Fig. 6) determine their contribution to the total system impedance. If the rate of the fast reaction is very high relative to the rate of the parallel slow reaction, i.e. $R_2 \ll R_3$, then the R_3 element would hardly contribute to the system impedance and its value will be non-definable. In that case the equivalent circuit shown in Fig. 5b would better characterise the system.

If the rate of charge transfer is small in comparison to the rate of diffusion then diffusion impedance is negligible in series connection with R_2. If there is no Warburg element two resistors are no longer distinguishable and are represented by one element forming an equivalent circuit shown in Fig. 5c.

Fig. 7 shows the dependencies of the parameters mentioned above on the potential for **m-MTDATA** oxidation. R_1 is not changing noticeably, as was expected, because this element is not related to the kinetics of the process. Dependencies of double layer capacitance (C), inverse charge transfer resistance R_2^{-1} (i.e. charge transfer conductivity) and inverse Warburg constant A_W^{-1} have a characteristic peak at potential 0.08 V, indicating that at this potential the system impedance is minimal. We present inverted plots of the charge transfer resistance and the Warburg constant because in that case maximums are more evident than minimums in direct plots. The R_3 value was very high (more than 10^6 Ω) and in some points could not be determined with satisfactory precision.

Fig. 8 shows the dependencies of the equivalent electrical circuit parameters calculated in a region of possible **m-MTDATA** reduction. This is a case of charge transfer limited reaction and the experimental spectra successfully fitted an equivalent circuit composed of three elements (Fig. 5c). The charge transfer conductance (R_2^{-1}) rises exponentially as the potential is decreased. However it no considerable difference in case of presence and absence of investigated compound was detected. The charge transfer conductivity (Fig. 5c) in presence of MTDATA was only three times higher than the conductivity of solvent. This negligible difference is not sufficient for precise estimation of the redox constant. It may be caused by error of charge transfer or zero potential determination. This dependence will be applied to estimate the redox constant.

Nevertheless, for a number of compounds a reduction behavior could be detected. Fig. 9 shows results of impedance analysis if TPBi reduction process.

In case of **TPBi** the first equivalent circuit (Fig. 5a) was applied to describe. An additional parallel resistance R_3 (Fig. 5a) was necessary to describe side-processes involving reduction products and the solvent (Fig. 6).

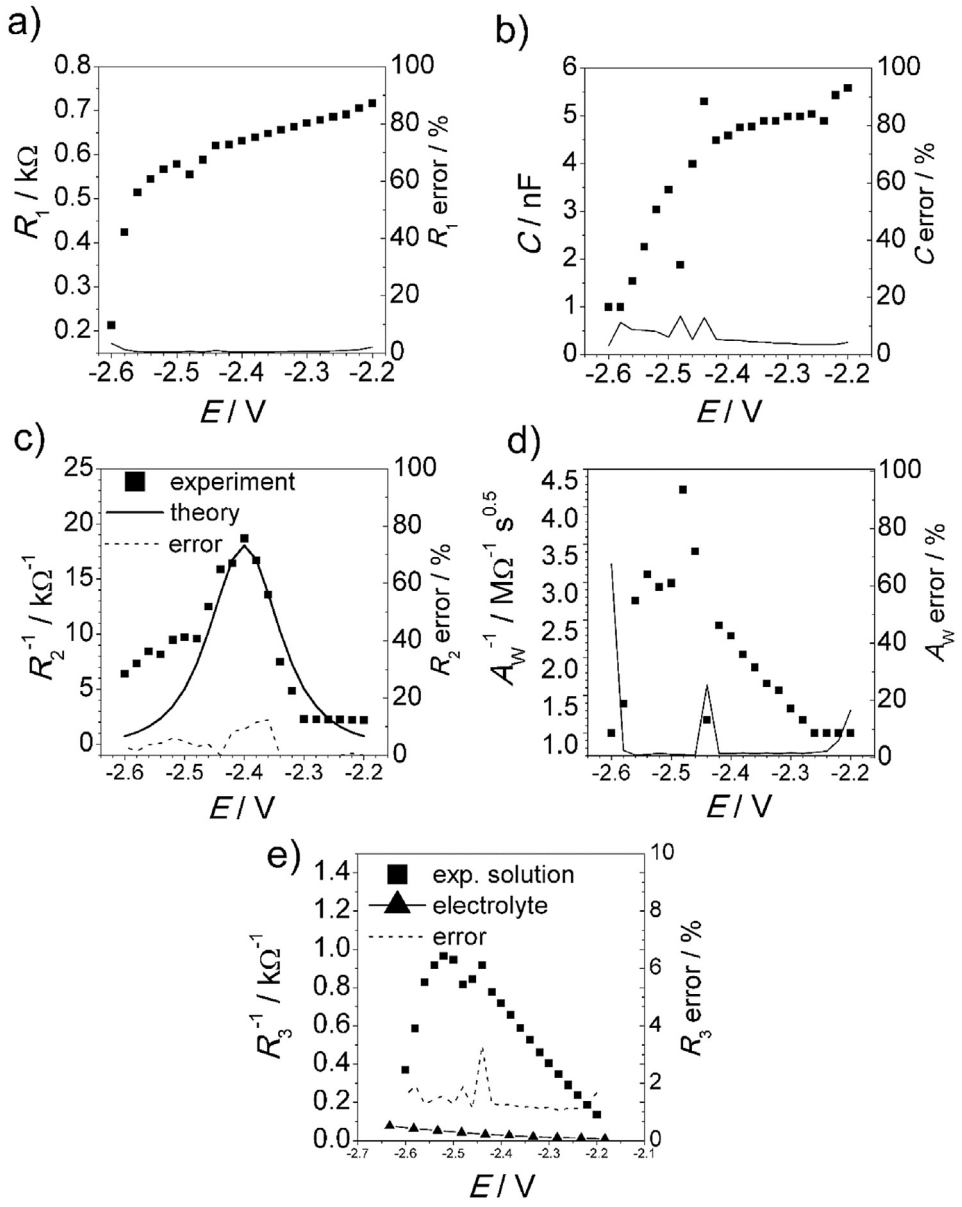

Fig. 9. Equivalent circuit parameters: R_1 (a), C (b), R_2^{-1} (c), A_W^{-1} (d), R_3^{-1} (e), their errors and fitting theoretical curves (c) corresponding to **TPBi** reduction as functions of electrode potential.

Figs. 10 and 11 present analogous plots of the equivalent circuit parameters characterising the oxidation and reduction of compound **V**, respectively.

In the case of **V** all the spectra fitted a simplified equivalent circuit shown in Fig. 5b because of the considerable prevalence of reversible charge transfer rate in respect to the irreversible one.

3.2. Calculation of the standard rate constant from impedance data

The derivation of the formulas used in this work is presented in fundamental books devoted to electrochemical impedance spectroscopy and electrochemical kinetics [21–24]. The charge transfer resistance R_{ct} depends on electroactive species surface concentrations (c_O^S and c_R^S) and forward and backward rate constants (k_c and k_a) according to (1):

$$R_{ct} = \frac{RT}{z^2F^2A}\frac{1}{\alpha k_c c_O^S + (1-\alpha)k_a c_R^S}, \quad (1)$$

where α is charge transfer coefficient ($0 < \alpha < 1$), A – electrode surface area. Rate constants are functions of potential according to the Butler-Volmer equation (2).

$$k_c = k^0 \cdot e^{-\alpha\frac{zF}{RT}(E-E^0)} \quad (2a)$$

$$k_a = k^0 \cdot e^{(1-\alpha)\frac{zF}{RT}(E-E_0)} \quad (2b)$$

where k^0 is the standard rate constant, E_0 is equilibrium potential, E is electrode potential. Stationary surface concentrations can be found from solution of Fick's partial differential equation [24].

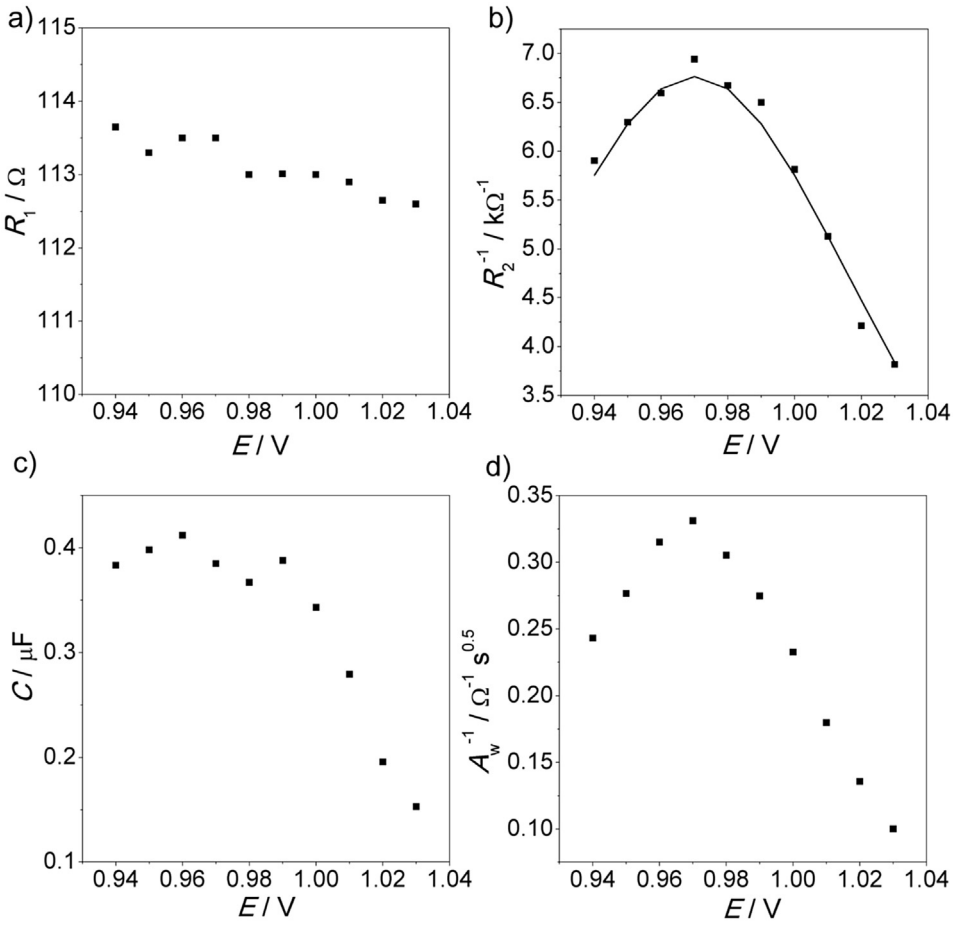

Fig. 10. Equivalent circuit parameters: R_1 (a), R_2^{-1} (b), C (c), A_W^{-1} (d) corresponding to **V** oxidation as functions of potential. Equivalent circuit and the corresponding element are shown in the insets.

$$c_O^s = \theta \frac{\xi c_O^b + c_R^b}{1 + \xi\theta} \tag{3a}$$

$$c_O^s = \frac{\xi c_O^b + c_R^b}{1 + \xi\theta} \tag{3b}$$

where c_O^b, c_R^b are bulk concentrations, ξ is a ratio of diffusion coefficients (D_O and D_R) (4) and θ is potential exponential function (5).

$$\xi = \sqrt{\frac{D_O}{D_R}} \tag{4}$$

$$\theta = e^{\frac{zF}{RT}(E - E_0)} \tag{5}$$

Substituting (2) – (5) into (1) one gets (6)

$$R_{ct}^{-1} = k^0 \frac{z^2 F^2 c_\Sigma}{RT} \frac{\theta^{1-\alpha}}{1+\theta} \tag{6}$$

A plot of the function (6) is a bell curve having the same form as the experimental points (Figs. 7b, 9b and 10b). Theoretical function (6) was fitted to the experimental data by tuning values of E_0, k^0 and α; the latter was accepted as being equal 0.5. It allowed adjustment of the equilibrium potential E_0 and an estimation of standard electrochemical rate constant k^0. Potential E_0 is easily determined as a potential at the maximum on the R_2^{-1}-E plot (Figs. 7b, 9c and 10b, Fig. 11b).

Considering graph of the theoretical function (6) and its parameters one can easily describe effect of each of them on the form of a graph. Changing E_0 shifts the whole curve along abscises scale. Changing k^0 controls height of the peak. Changing z would cause modification of peak sharpness as demonstrated in Fig. 7b. Coefficient α regulates symmetry of the peak (at $\alpha = 0.5$ both peak shoulders are equal). An attempt to fit all four parameters with experimental data lead to non-realistic values of α due to non-ideality of real electrochemical system. For that reason α was fixed at 0.5. The value of z, when calculated from fitting results, ranged from 0.9 to 1.1. Therefore it was also fixed to be 1.0, two parameters E_0 and k^0 remaining unknown and easy to be calculated.

If the reaction is irreversible then the functions (1) and (6) are modified taking into account the presence of a sole process. It resulted in omitting one of the terms in the denominator in formula (6) (either θ or 1). Thus formula (6) was transformed to (7) and (8) for oxidation and reduction processes, respectively. E.g. formula (8) was used for fitting experimental data in Fig. 8 c.

$$R_{ct}^{-1} = k^0 \frac{z^2 F^2 c_\Sigma}{RT} \theta^{1-\alpha} \tag{7}$$

$$R_{ct}^{-1} = k^0 \frac{z^2 F^2 c_\Sigma}{RT} \theta^{-\alpha} \tag{8}$$

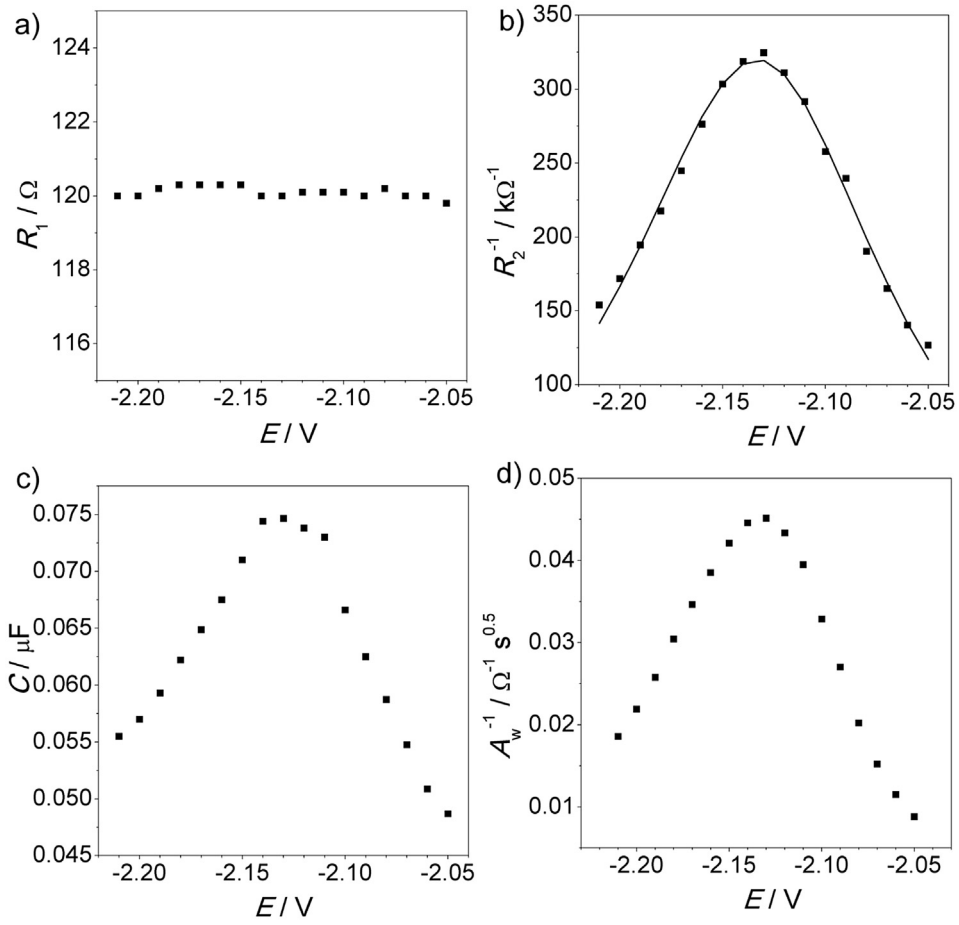

Fig. 11. Equivalent circuit parameters: R_1 (a), R_2^{-1} (b), C (c), A_W^{-1} (d) corresponding to **V** oxidation as functions of potential. Equivalent circuit and the corresponding element are shown in the insets.

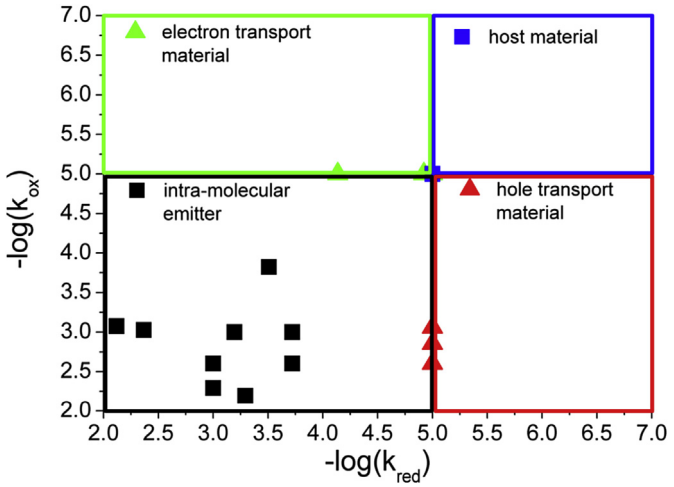

Fig. 12. Comparison of redox standard rate constants of the investigated compounds: hole, electron-transport and host materials (Table 1), intra-molecular exciplex emitters (Table 2). Coloured rectangles designate areas corresponding to roles of the compounds play in diodes.

The calculated values of charge transfer rate constants of all the investigated substances are presented in Tables 1 and 2

Obviously rate constant estimated from formula (8) is strongly dependent on the value of equilibrium potential. In several cases a value calculated from the reference LUMO data can be used. The reference investigation of a solution containing only electrolyte was carried out in order to estimate a minimal limit of measurable kinetic constant. Figs. 8c and 9e show charge transfer conductivity plots overlapped with plots obtained in presence of investigated compounds. The apparent redox rate constant referred to the solvent was found to be $4.3 \cdot 10^{-6}$ if the reduction potential assumed to be −2.9 V. We regarded that value as a limit for distinguishing the response of a process involving the investigated molecule from a background signal. Since there was no evidence of occurring redox process one can regard it neither not to take place or to be very slow (rate constant $< 1 \cdot 10^{-5}$) to be detected by the impedance method.

On the other hand, rate constants of a very fast charge transfer reaction could not be estimated precisely because in that case the reaction was limited by diffusion. Charge transfer resistance was very small in comparison to diffusion impedance. The higher limit of possible redox constant value was estimated to be $1 \cdot 10^{-2}$. For that reason values which are estimated to be very high are shown in Table 2 as $> 1 \cdot 10^{-2}$. Fig. 12 presents the resulting data from Tables 1 and 2 in a graphical mode. Negative decimal logarithms ($pk = -\log(k)$) of reduction and oxidation rate constants correspond to abscissa and ordinate of the points, respectively. The approximate regions corresponding to different roles of the compounds are shown on the graph by coloured rectangles.

Kinetic constants that could not be determined were attributed values of $1 \cdot 10^{-5}$ m·s^{-1} to depict on a graph as a minimal value that could be estimated for compound in solution. The real value of a

constant must be lower so that the point related to the compound would find it self in the corresponding rectangle region (Fig. 12). All the compounds including both donor and acceptor molecule units (Table 2) are characterised by much higher both oxidation and reduction rate constants than the other pure donor or acceptor compounds (Table 1). Rate constants of the D-A-D compounds exceed the rate constants of single donor or acceptor molecules (Table 1) by 2-3 orders. Thus the presence of both donor and acceptor parts together in one molecule enhances the molecule's ability to exchange charge rapidly in both oxidation and reduction directions. Secondly, the ratios of oxidation and reduction rate constants of hole- and electron-transport compounds correlate with their conductivity types although the redox rate constant and the charge carrier mobility refer to different phases (solution and solid). This correlation may be used for prediction of the behaviour of a compound in the solid state based on its behaviour in solution. If a compound is oxidised faster than it is reduced, then charge in the solid state would be predominantly transferred by reversible oxidation, i.e. by M^+/M-states (M = molecule), which means hole-type transport. The opposite case, where charge is predominantly exchanged due to reversible reduction, i.e. between M/M^--state, means electron-type transport. Oxidation rate constants of hole-transport materials were found to be higher than oxidation rate constants of electron-transport materials (Fig. 12, Table 1). The same statement can be made in relation to the electron-transport materials and reduction rate constants. The other feature which deserves attention is the very low values of the reduction rate constants. Their values are not only very small, but also they do not differ significantly even between hole- and electron-transport compounds. This means that all the organic compounds under investigation reduce more slowly than they oxidise. This result corresponds to a known fact that hole mobility in organic solid films is in most cases much higher than electron mobility [25,26]. Finally, the compounds used as host materials were found to be oxidised and reduced very slowly and irreversibly. Therefore, their rate constants could not be estimated.

4. Conclusions

The choice of a compound for a specific role in an OLED is predominantly based on its relative orbital energy levels and its emission spectrum. In this work we have thrown light upon another important aspect – namely, the conductivity properties of an organic material and an easy way to predict these properties by analysis in solution.

The proposed impedance-based technique has proved to be effective for the characterisation of thermodynamic (HOMO and LUMO levels) and kinetic (redox rate constants) parameters of a wide variety of molecules used in OLEDs. Although no direct relationship between structure and numerical data could be revealed, several particular aspects were elucidated:

(i) the redox rate of ambipolar compounds containing donor and acceptor parts appeared much higher than those of pure donors and acceptors. The rise of rate is very important for organic electronics and electrochromic devices. In the electrochromic devices, it will decrease switching time, current and the possibility of degradation. In the organic electronic devices, it may influence change balance and recombination rate within the active component;

(ii) the relationship between oxidation and reduction rate constants is responsible for the compound's conductivity type in the solid state and is expected to be an easy tool to predict compound performance when incorporated in an OLED-layer.

Acknowledgements

The authors gratefully acknowledge financial support of “Exci-light” project “Donor-Acceptor Light Emitting Exciplexes as Materials for Easy-to-tailor Ultra-efficient OLED Lightning” (H2020-MSCA-ITN-2015/674990) funded by Marie Skłodowska-Curie Actions within the framework programme for research and innovations “Horizon-2020”. J.S. and M.R.B. thank EPSRC grant number EP/L02621X/1 for funding.

Appendix A. Supplementary data

Supplementary data related to this article can be found at https://doi.org/10.1016/j.electacta.2017.11.171.

References

[1] Organic electronics, ChemPhysChem 16 (2015) 1097–1305.
[2] J. Pei, W.-L. Yu, J. Ni, Y.-H. Lai, W. Huang, A.J. Heeger, Thiophene-based conjugated polymers for light-emitting Diodes: effect of Aryl groups on photoluminescence efficiency and redox behavior, Macromolecules 34 (2001) 7241.
[3] M. Lapkowski, P. Data, S. Golba, J. Soloducho, A. Nowakowska-Oleksy, Unusual band-gap migration of N-alkylcarbazole-thiophene derivative, Opt. Mater 22 (2011) 1445.
[4] S. Trasatti, The absolute electrode potential: an explanatory note, Pure Appl. Chem. 58 (1986) 955.
[5] P. Data, M. Lapkowski, R. Motyka, J. Suwinski, Influence of heteroaryl group on electrochemical and spectroscopic properties of conjugated polymers, Electrochim. Acta 83 (2012) 271.
[6] P. Data, P. Pander, M. Lapkowski, A. Swist, J. Soloducho, R.R. Reghu, J.V. Grazulevicius, Unusual properties of electropolymerized 2,7-and 3,6-carbazole derivatives, Electrochim. Acta 128 (2014) 430.
[7] J.L. Bredas, Mind the gap!, Mater. Horiz. 1 (2014) 17.
[8] M. Etherington, F. Franchello, J. Gibson, T. Northley, J. Santos, J. Ward, H. Higginbotham, P. Data, A. Kurowska, P. Santos, D. Graves, A.S. Batsanov, F. Dias, M.R. Bryce, T. Penfold, A. Monkman, Regio- and conformational isomerization critical to design of efficient thermally-activated delayed fluorescence emitters, Nat. Commun. (2017), https://doi.org/10.1038/ncomms14987.
[9] F.B. Dias, J. Santos, D. Graves, P. Data, R. Nobuyasu, M.A. Fox, T. Palmeira, M. Berberan-Santos, M.R. Bryce, A. Monkman, The role of local triplet excited states in thermally-activated delayed fluorescence: photophysics and devices, Adv. Sci. 3 (2016) 1600080.
[10] V. Jankus, P. Data, D. Graves, C. McGuinness, J. Santos, M.R. Bryce, F.B. Dias, A.P. Monkman, Highly efficient TADF OLEDs: how the emitter–host interaction controls both the excited state species and electrical properties of the devices to achieve near 100% triplet harvesting and high efficiency, Adv. Funct. Mater. 24 (2014) 6178.
[11] F. Dias, K. Bourdakos, V. Jankus, K. Moss, K. Kamtekar, V. Bhalla, J. Santos, M.R. Bryce, A.P. Monkman, Triplet harvesting with 100% efficiency by way of thermally activated delayed fluorescence in charge transfer OLED emitters, Adv. Mater. 25 (2013) 3707.
[12] P. Data, R. Motyka, M. Lapkowski, J. Suwinski, S. Jursenas, G. Kreiza, A. Miasojedovas, A.P. Monkman, Efficient p-phenylene based OLEDs with mixed interfacial exciplex emission, Electrochim. Acta 182 (2015) 524.
[13] P. Data, A. Swist, M. Lapkowski, J. Soloducho, K. Darowicki, A.P. Monkman, Evidence for solid state electrochemical degradation within a small molecule OLED, Electrochim. Acta 184 (2015) 86.
[14] V. Jankus, Ch-J. Chiang, F. Dias, A.P. Monkman, Deep blue exciplex organic light-emitting diodes with enhanced efficiency; P-type or E-type triplet conversion to singlet excitons? Adv. Mater. 25 (2013) 1455.
[15] P. dos Santos, J. Ward, M.R. Bryce, A.P. Monkman, Using guest host interactions to optimise the efficiency of TADF-OLEDs, J. Phys. Chem. Lett. 7 (2016) 3341.
[16] K. Goushi, K. Yoshida, K. Sato, C. Adachi, Organic light-emitting diodes employing efficient reverse intersystem crossing for triplet-to-singlet state conversion, Nat. Photonics 6 (2012) 253.
[17] J. Wang, J. Gou, W. Li, Phosphorescent molecularly doped light-emitting diodes with blended polymer host and wide emission spectra, Sci. World J. (2013), 954146, **2013**, 5, doi: 10.1155/2013/954146.
[18] M. Wong, E. Zysman-Colman, Purely organic thermally activated delayed fluorescence materials for organic light-emitting diodes, Adv. Mater. (2017), https://doi.org/10.1002/adma.201605444.
[19] Y.J. Cho, K.S. Yook, J.Y. Lee, High efficiency in a solution-processed thermally activated delayed-fluorescence device using a delayed-fluorescence emitting material with improved solubility, Adv. Mater. 26 (2014) 6642.
[20] G. A. Ragoisha, A. S. Bondarenko, EIS spectrum analyser. http://www.abc.chemistry.bsu.by/vi/analyser.
[21] E. Barsoukov, J.R. Macdonald, Impedance Spectroscopy: Theory, Experiment, and Applications, second ed., Wiley, 2005.

[22] M.E. Orazem, B. Tribollet, Electrochemical Impedance Spectroscopy, Wiley, 2008.
[23] A. Lasia, Electrochemical Impedance Spectroscopy and its Applications, Springer, 2014.
[24] A.J. Bard, L.R. Faulkner, Electrochemical Methods: Fundamentals and Applications, second ed., Wiley, 2001, p. 864.
[25] W. Brütting, S. Berleb, A.G. Mückel, Device physics of organic light-emitting diodes based on molecular materials, Org. Electron 2 (2001) 1.
[26] S. Nowy, W. Ren, A. Elschner, W. Lövenich, W. Brütting, Impedance spectroscopy as a probe for the degradation of organic light-emitting diodes, J. Appl. Phys. 107 (2010), 054501.